

Close-to-fission dumbbell Jupiter-Trojan (17365) Thymbraeus

B. Carry¹, P. Descamps², M. Ferrais³, J.-P. Rivet¹, J. Berthier², E. Jehin⁴, D. Vernet⁵, L. Abe¹, P. Bendjoya¹,
F. Vachier², M. Pajuelo^{2,6}, M. Birlan^{2,7}, F. Colas², and Z. Benkhaldoun⁸

¹ Université Côte d'Azur, Observatoire de la Côte d'Azur, CNRS, Laboratoire Lagrange, France e-mail: benoit.carry@oca.eu

² IMCCE, Observatoire de Paris, PSL Research University, CNRS, Sorbonne Universités, UPMC Univ Paris 06, Univ. Lille, France

³ Arecibo Observatory, University of Central Florida, HC-3 Box 53995, Arecibo, PR 00612, USA

⁴ Space sciences, Technologies and Astrophysics Research (STAR) Institute, Université de Liège, Allée du 6 Août 17, 4000 Liège, Belgium

⁵ Université Côte d'Azur, Observatoire de la Côte d'Azur, CNRS, UAR Galilée, France

⁶ Sección Física, Departamento de Ciencias, Pontificia Universidad Católica del Perú, Apartado 1761, Lima, Perú

⁷ Astronomical Institute of the Romanian Academy, Cutitul de argint -5, sector 4, Bucharest, Romania

⁸ Oukaimeden Observatory, High Energy Physics and Astrophysics Laboratory, Cadi Ayyad University, Marrakech, Morocco

Received X; accepted Y

ABSTRACT

Context. Every population of small bodies in the Solar system contains a sizable fraction of multiple systems. Among these, the Jupiter Trojans have the lowest number of known binary systems and the least characterized.

Aims. We aim at characterizing the reported binary system (17365) Thymbraeus, one of the only seven multiple systems known among Jupiter Trojans.

Methods. We conducted light curves observing campaigns in 2013, 2015, and 2021 with ground-based telescopes. We model these lightcurves using dumbbell equilibrium figures.

Results. We show that Thymbraeus is unlikely a binary system. Its light curves are fully consistent with a bilobated shape: a dumbbell equilibrium figure. We determine a low density of $830 \pm 50 \text{ kg.m}^{-3}$, consistent with the reported density of other Jupiter Trojan asteroids and small Kuiper-belt objects. The angular velocity of Thymbraeus is close to fission. If separated, its components would become a similarly-sized double asteroid such as the other Jupiter Trojan (617) Patroclus.

1. Introduction

The small bodies with satellites represent a highly diverse population in the Solar system, spanning a wide range of diameter, separation, and size ratio (Figure 1, and Margot et al., 2015, for a review). Some systems are made of large and similarly-sized bodies. These double systems are thought to be primordial and are abundant in the Kuiper belt (Fraser et al., 2017). The largest small bodies (diameters above a 100 km typically) can also have small satellites, believed to form from the re-accumulation of ejecta after impacts, found in both the asteroid and the Kuiper belt (e.g., Ragozzine & Brown, 2009; Berthier et al., 2014; Carry et al., 2019, 2021; Vachier et al., 2022). An abundant population (about 15%, Margot et al., 2002; Pravec et al., 2006) of small asteroids (diameter below 10 km) have close-in satellites, likely produced by fission due to YORP spin-up (Walsh et al., 2008; Walsh & Jacobson, 2015; Zhang et al., 2022).

As of today, the least characterized population of small bodies in term of multiplicity are the Jupiter Trojans. Only seven multiple systems have been discovered: (617) Patroclus from Gemini (Merline et al., 2001), (624) Hektor from W. M. Keck (Marchis et al., 2006), (3548) Eurybates with the Hubble Space Telescope (HST, Noll et al., 2020), (15094) Polymele by stellar occultation (Buie et al., 2022), (16974) Iphigeneia with the HST (Noll et al., 2016), and both (17365) Thymbraeus and (29314) Eurydamas from light curves (Mann et al., 2007). This low number of binary systems is most-likely the result of observing biases. Radar observations efficient in discovering satellites are limited in range (Benner et al., 2015), adaptive-optics observations require a bright source and have been mainly limited

to large main-belt asteroids (and the brightest KBOs, Merline et al., 1999; Marchis et al., 2005; Carry et al., 2011; Yang et al., 2020). While the HST does not require a bright source, most studies focused on KBOs (Noll et al., 2004; Brown et al., 2006; Grundy et al., 2011) until the selection of the Lucy mission by NASA (Levison et al., 2017). Finally, while the majority of binaries have been discovered by light curves (see Johnston, 2018), often by amateur astronomers, the Jupiter Trojans are faint for most amateur equipment (Mousis et al., 2014).

However, Jupiter Trojans are a unique population, related to the outer Solar system, and trapped on the L4/L5 Lagrangian points of the Sun-Jupiter system during the phase of dynamical instability in the early Solar system (Morbidelli et al., 2005; Nesvorný et al., 2018). We focus here on the reported binary (17365) Thymbraeus¹. We conducted an observing campaign spanning several oppositions to determine the physical properties of this object.

The article is organized as following. In Section 2 we present the observations and data reduction. We describe how we determine the properties of Thymbraeus in Section 3, and discuss their implications in Section 4.

2. Observations

We observed Thymbraeus in 2015 on seven dates with the 104 cm Omicron telescope of the Centre Pédagogique Planète et Univers (C2PU) facility (Bendjoya et al., 2012) located at the Calern observing site (Côte d'Azur Observatory, France, IAU

¹ Formerly 1978 VF11

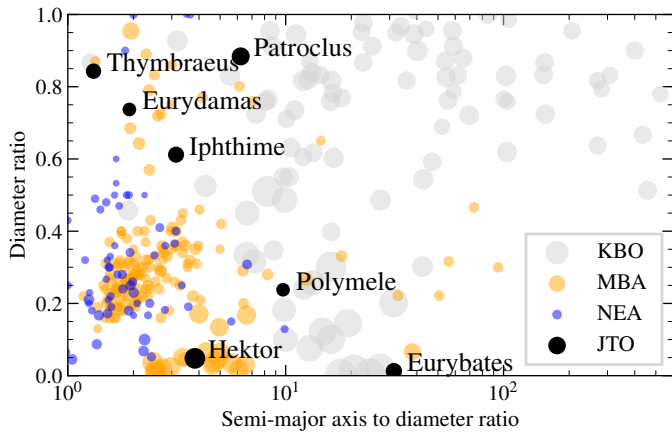


Fig. 1: The diversity among small body binaries, with the seven known Jupiter Trojans (JTO) in black. The satellite diameters and semi-major axes are from [Johnston \(2018\)](#) and the diameters of the primary bodies from the SsODNet service ([Berthier et al., 2023](#)).

code: 010). In 2021, we used three facilities. We collected 29 epochs with the 60 cm André Peyrot telescope mounted at Les Makes observatory (IAU code 181) on La Réunion Island. We finally acquired 15 and 5 epochs with the TRAPPIST south and north telescopes (IAU code I40 and Z53, respectively, [Jehin et al., 2011](#)). For all these observations, standard reduction (dark subtraction, flat-fielding) and photometry procedure (plate solution, zero point, aperture photometry) was conducted. We also retrieved the four light curves obtained in 2013 by [Stephens et al. \(2014\)](#) with a 40 cm telescope in his observatory (IAU code U81), available on ALCDEF² ([Warner, 2016](#)). The detailed logs of observations are provided in [Table 1](#). Photometric uncertainties are estimated to about 0.03 mag from their scatter.

We complement this data set with the observations from 2005 and 2006 reported by [Mann et al. \(2007\)](#) that we digitized. These last two light curves were only plotted in the article and not available in tabular format. Furthermore, these were reported as function of the rotation phase and in reduced magnitude, not as observed (epoch, magnitude). We thus do not use these two light curves for modeling but as a posteriori validation of the solution.

3. Analysis

3.1. Synodic period

We use the Phase Dispersion Minimization (PDM) technique ([Stellingwerf, 1978](#)) to search for the synodic rotation period within the photometric data (all epochs are lighttime corrected). We assume here that two maxima and minima occur per rotation. Based on a trial period, PDM bins data according to the rotational phase. The average variance of these subsets is compared to the overall variance of the full set of observations. It defines the statistical parameter θ . The best estimate of the period is the one which minimises θ . This method does not assume any sinusoidal variation of the light curve and is well suited for unevenly spaced observations. PDM finds all periodic components or subharmonics (aliases of the period). We follow the approach used by [Berthier et al. \(2020\)](#) for (617) Patroclus: we first determine the synodic period with PDM for each epoch of

Table 1: Log of observations.

Date	Telescope	Duration	N	V (mag)	α (°)
2013-09-28	U81	6h52	69	17.7	8.0
2013-09-29	U81	6h26	48	17.7	7.9
2013-10-02	U81	6h17	63	17.6	7.4
2013-10-03	U81	7h16	55	17.6	7.2
2015-11-23	010	2h00	24	18.2	9.0
2015-11-25	010	6h20	74	18.2	8.7
2015-12-16	010	3h15	39	17.9	5.7
2015-12-16	010	3h25	41	17.9	5.7
2015-12-19	010	4h25	53	17.9	5.2
2015-12-20	010	1h55	23	17.9	5.0
2015-12-21	010	7h50	94	17.9	4.8
2021-05-14	Z53	1h27	43	17.9	4.6
2021-05-15	I40	4h22	91	17.9	4.4
2021-05-17	I40	8h26	97	17.9	4.0
2021-05-17	181	6h42	46	17.9	4.0
2021-05-18	181	3h47	39	17.9	3.8
2021-05-22	181	1h48	6	17.8	3.1
2021-05-23	I40	3h40	46	17.8	2.9
2021-05-24	I40	3h31	41	17.8	2.7
2021-05-24	181	2h06	22	17.8	2.7
2021-05-25	I40	2h45	34	17.8	2.5
2021-05-29	181	4h05	31	17.7	1.7
2021-05-30	181	2h42	28	17.7	1.5
2021-05-30	I40	3h56	43	17.7	1.5
2021-05-31	181	4h24	38	17.7	1.3
2021-06-02	181	3h30	38	17.6	0.9
2021-06-03	181	3h30	35	17.6	0.7
2021-06-06	181	2h47	16	17.5	0.2
2021-06-07	181	1h36	14	17.5	0.2
2021-06-07	I40	3h35	52	17.5	0.2
2021-06-07	I40	7h41	88	17.5	0.2
2021-06-08	181	5h00	27	17.6	0.4
2021-06-09	181	2h17	17	17.6	0.5
2021-06-09	Z53	2h04	28	17.6	0.5
2021-06-10	181	5h42	20	17.6	0.7
2021-06-12	181	7h24	43	17.7	1.1
2021-06-13	181	6h54	41	17.7	1.3
2021-06-14	181	4h24	17	17.7	1.5
2021-06-15	181	3h42	17	17.7	1.7
2021-06-17	181	6h17	33	17.7	2.1
2021-06-19	181	3h06	19	17.8	2.5
2021-06-26	181	0h54	11	17.9	3.9
2021-06-27	181	5h30	37	17.9	4.1
2021-06-29	181	5h47	40	17.9	4.4
2021-06-29	I40	8h18	109	17.9	4.4
2021-06-29	Z53	1h48	31	17.9	4.4
2021-07-01	I40	4h54	69	17.9	4.8
2021-07-02	181	3h42	23	17.9	5.0
2021-07-04	Z53	2h17	40	18.0	5.3
2021-07-04	181	4h17	26	18.0	5.3
2021-07-08	Z53	2h15	32	18.0	6.0
2021-07-25	181	3h06	30	18.2	8.4
2021-07-26	181	4h05	31	18.2	8.6
2021-07-30	181	1h00	9	18.3	9.0
2021-08-02	I40	4h00	57	18.3	9.3
2021-08-03	181	0h54	9	18.3	9.4
2021-08-03	I40	4h54	70	18.3	9.4
2021-08-06	I40	3h39	53	18.3	9.7
2021-08-12	I40	5h15	75	18.4	10.1
2021-08-27	I40	4h42	68	18.5	10.8

² <https://alcdef.org/>

observation: 2013, 2015 and 2021. We then search for the fundamental synodic period by combining all epochs, and find $P_{\text{syn}} = 12.671575 \pm 0.000003$ h.

3.2. Spin-vector coordinates

From the change of shape of the light curves collected in 2013, 2015 and 2021, we determine a set of two symmetric pole solutions. We therefore solve the following system which gives the position of the rotation pole from simple and relevant assumptions on the latitude of the sub-observer point (Descamps et al., 2007). The latitude of the sub-observer point (β_{SEP}) and the North pole position angle (n_p) are related to the equatorial coordinates of the rotation pole (α_0, δ_0) and the equatorial coordinates of the asteroid (α, δ) for each epoch by the following equations :

$$\begin{aligned} \sin \beta_{\text{SEP}} &= -\sin \delta_0 \sin \delta - \cos \delta_0 \cos \delta \cos(\alpha - \alpha_0) \\ \sin n_p \cos \beta_{\text{SEP}} &= -\cos \delta_0 \sin(\alpha - \alpha_0) \\ \cos n_p \cos \beta_{\text{SEP}} &= \sin \delta_0 \cos \delta - \cos \delta_0 \sin \delta \cos(\alpha - \alpha_0) \end{aligned} \quad (1)$$

The search for possible solutions for the rotation pole of the asteroid is mainly based on assumptions concerning the latitude of the sub-observer point. These are constrained by the observed amplitudes of the light curves. The light curve observed in 2013 is the one with the lowest amplitude, 0.76 mag. That of 2015, conversely, presents the largest amplitude, 1.16 mag. Finally, that of 2021 still shows a significant amplitude although smaller than in 2015. From these findings we formulate the following assumptions : in 2013, $|\beta_{\text{SEP}}| > 14^\circ$; in 2015, $|\beta_{\text{SEP}}| < 4^\circ$; in 2021, $|\beta_{\text{SEP}}| < 10^\circ$.

We consider the two following observation pairs : 2013/2021 and 2015/2021. For each pair, we search graphically for the areas of the solution space for which the previous conditions on the latitude of the sub-observer point are satisfied. Each pair of subterrestrial latitude values for each epoch point is defined on a grid of values from -16° to $+16^\circ$ with a step of 0.5° (Figure 2).

In order for the above conditions to be satisfied, it is necessary to select the solutions that are at the intersection of the red area for the 2013/2021 epoch (Figure 2, left) and the blue area for the 2015/2021 epoch (Figure 2, right). We can then infer two symmetrical pole solutions (direct and retrograde), they are visualized on Figure 2 with a black cross. The J2000 equatorial coordinates of the pole 1 are $\alpha_0 = 92 \pm 2^\circ$ and $\delta_0 = -77 \pm 2^\circ$. The solution for the pole 2 is given by $\alpha_0 = 268 \pm 2^\circ$ and $\delta_0 = +77 \pm 2^\circ$.

3.3. Shape

High brightness variations (greater than 0.9 mag), U-shaped maxima and V-shaped minima are convincingly suggestive of an elongated shape with two lobes at the ends separated by a narrower neck (Descamps, 2015). In a previous study devoted to the Trojan asteroid Thymbraeus (Mann et al., 2007), the authors sought to model their photometric light curves using two tightened and doubly synchronized equilibrium Roche ellipsoids. The aim was to determine how well the observations could be matched by theoretical light curves of a bilobated shape.

However, Gnat & Sari (2010) showed that equilibrium figures of tightly bound binaries are no longer triaxial ellipsoids, and departures from the pure ellipsoidal forms may amount to nearly 20%. They found that at mutual separation on the order of twice the sum of their mean radius, departures from ellipsoids

given by the Roche binary approximation are negligible. On the other hand, Descamps (2015) showed two Roche ellipsoids only provided an approximation to the properties of a bilobated object, while dumbbell-shaped equilibrium figures provide numerical solution without bias on the angular momentum. In such case, the solution is entirely described by a single parameter, the normalized angular velocity Ω defined by the ratio between the angular frequency ω and the critical spin rate for a spherical body ω_c , which is the maximum spin rate that can be sustained by a rigid body :

$$\Omega = \frac{\omega}{\omega_c} = \omega \sqrt{\frac{4}{3} \pi \rho G} \quad (2)$$

where G is the gravitational constant, and ρ the bulk density.

Therefore, we investigate here a more reliable shape solution belonging to the dumbbell equilibrium sequence. The objects of this sequence are symmetric with respect to one axis and rotate around a second axis perpendicular to the symmetry axis. The dumbbell sequence was first computed by Eriguchi et al. (1982) and more recently fully characterized by Descamps (2015). The synthetic light curves are produced taking into account the photometric effects induced by the scattering effects of sunlight by the surface of the object coupled to the phase angle. We present these lightcurves with the observations in Figure 3. The lightcurves agree well with observations (RMS residuals of 0.05, 0.12, 0.6 mag for the three epochs), while presenting some departures, likely due to surface features not represented by the dumbbell equilibrium figure. In addition, even at the small phase angles involved (8° in 2013, 6° in 2015 and 4° in 2021), it is necessary to take into account the significant effect of mutual shadowing. We adopted a scattering law combining through a weight factor k a lambertian icy-type law, suitable for high albedo surfaces, and a lunar-type reflection described by the Lommel-Seeliger law appropriate for low albedo surfaces (Kaasalainen et al., 2001). We adopt $k = 0.05$. The best-fit solution was obtained simultaneously with the determination of the sidereal periods for each pole solution: $\Omega = 0.285 \pm 0.01$, $P_{\text{sid},1} = 12.671821$ h and $P_{\text{sid},2} = 12.672607$ h. We determine a density of $\rho = 830 \pm 50 \text{ kg.m}^{-3}$ from the sidereal periods and the normalized angular velocity. This low density is similar to the density of $780_{-80}^{+50} \text{ kg.m}^{-3}$ originally reported by Mann et al. (2007), and typical of Trojans and similarly-sized KBOs (e.g., Carry, 2012; Scheeres et al., 2015) and suggests a porous interior characteristic of rubble piles.

The light curves present an asymmetry between the minima, noticeably apparent in 2013 with a magnitude differential of 0.05 mag. We thus apply a small perturbation to the hydrostatic equilibrium shape solution using a Gaussian random sphere (Muinonen, 1998) allowing to take into account substantial internal friction present in rubble pile objects (Descamps, 2016). In doing so, a so-called near-equilibrium shape is constructed by combining the initial dumbbell shape model with a Gaussian random sphere which approximates the departure with the real shape. Obviously, this does not mean that the resulting solution is the exact solution but just that the asymmetry between photometric minima may be interpreted by small shape deviations from a perfect fluid solution. We use a Gaussian random sphere generated by two parameters, the relative standard deviation of radial distance, $\sigma = 0.05$, and the input correlation angle of the Gaussian sphere, $\Gamma = 180^\circ$. The resulting object has the following statistical properties according to the notations introduced in Muinonen (1998) and Muinonen & Lagerros (1998): $\bar{\sigma}$

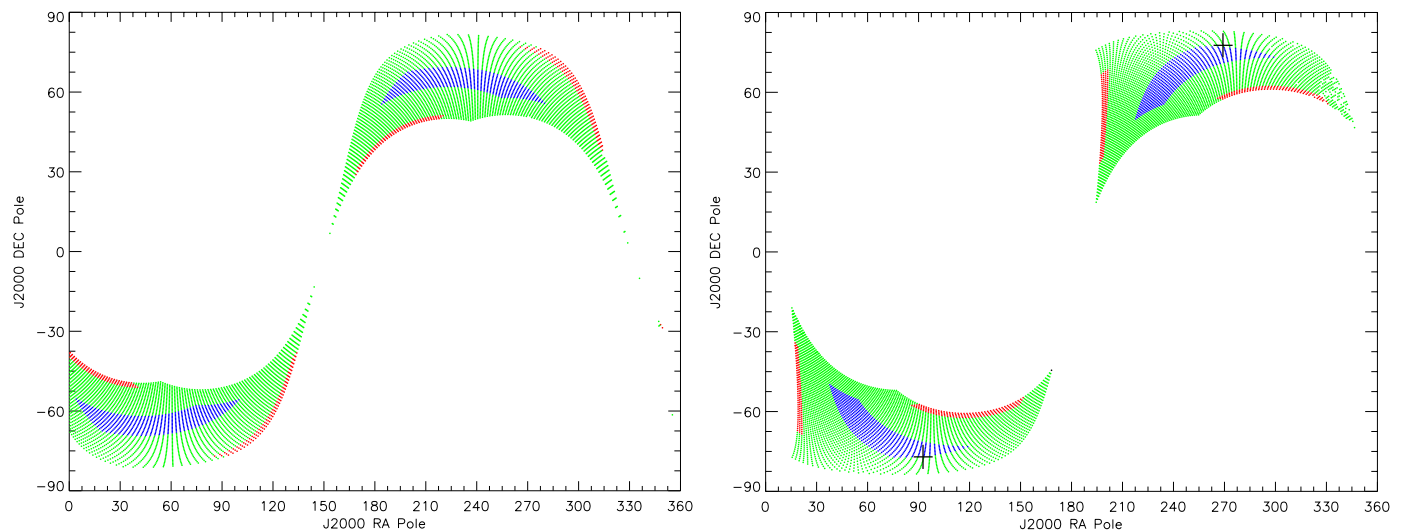


Fig. 2: Solution space for the pole of rotation for 2013/2021 (left) and 2015/2021 (right), see text. The black cross gives the solution intersection of the red and blue areas.

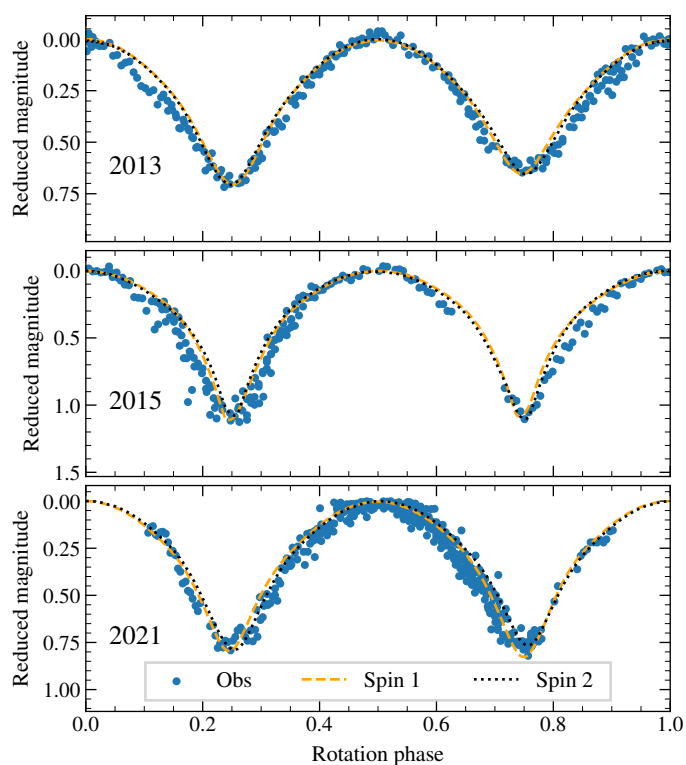


Fig. 3: Observed light curves of Thymbraeus compared with the synthetic light curves with the two spin solutions. The coordinates (α_0, δ_0) of the spin solutions are $(92^\circ, -77^\circ)$ and $(268^\circ, -77^\circ)$ for the Spin 1 and 2, respectively (see text).

$= 0.98$, $\tilde{\Gamma} = 56.9^\circ$, $\tilde{\rho} = 0.86$, and the standard deviation of shape angle, $\tilde{\Phi} = 40.8^\circ$.

The inferred estimated slope angle (assimilated to the angle of repose) is 2.5° . The angle of repose for a fluid body is, however, strictly zero. It is often pointed out that loosely consolidated piles of aggregated particles have slopes that are maintained at the angle of repose with respect to horizontal. We present in Figure 4 the final shape solution obtained for Thymbraeus.

Our model reproduces faithfully the observed light curves without invoking two Roche ellipsoids with a significant secondary-to-primary mass ratio as for the solution proposed by Mann et al. (2007). Our solution also reproduces the light curves observed in April 2005 and February 2006 and published in Mann et al. (2007), see Figure 5. The photometric ranges and the asymmetries between the minima are perfectly reproduced. Mann et al. (2007) assumed that the object was viewed equatorially in 2005 (aspect angle of 90° or $\beta_{\text{SEP}} = 0^\circ$), thus producing the larger photometric range of ~ 1 mag but at the cost of a differential drop between minima of nearly 0.1 mag. With the 2006 observations, they found that an aspect angle of 75° ($\beta_{\text{SEP}} = 15^\circ$) produced a better fit. Our solution gives respectively $\beta_{\text{SEP}} = -6^\circ$ in 2005 and $\beta_{\text{SEP}} = -10^\circ$ in 2006. Furthermore, if we do not take into account the effects of cast shadows, we obtain an amplitude of 0.917 mag in 2005 instead of 0.971 mag and with a quasi-absence of asymmetry (Figure 5). We also plot the synthetic light curves for different values of Ω . They show that the photometric range increases with Ω while the differential in magnitude decreases. This results from the fact that when Ω increases, the corresponding equilibrium figure of the dumbbell sequence elongates with a thickening of its waist. With the nominal solution $\Omega = 0.285$, the magnitude differential is $\Delta = 0.034$ mag, but for $\Omega = 0.300$, $\Delta = 0.017$ mag.

All the collected light curves so far do not show unequal minima, this tends to show that the two lobes are of similar size. If this were not the case, we would observe a differential in magnitude whatever the orientation of the system. This proves that the magnitude differential arises from a significant mutual shadowing between the lobes, differing one from the other by their shape but not by their size, under specific geometric configurations. This underlines the importance of taking into account all photometric effects including mutual shadowing which must be combined simultaneously with a reliable pole solution, independently derived from any consideration on the shape model, and a realistic shape solution.

4. Discussion

The dumbbell model had already been successfully applied to the asteroid (216) Kleopatra (Descamps, 2015), which was al-

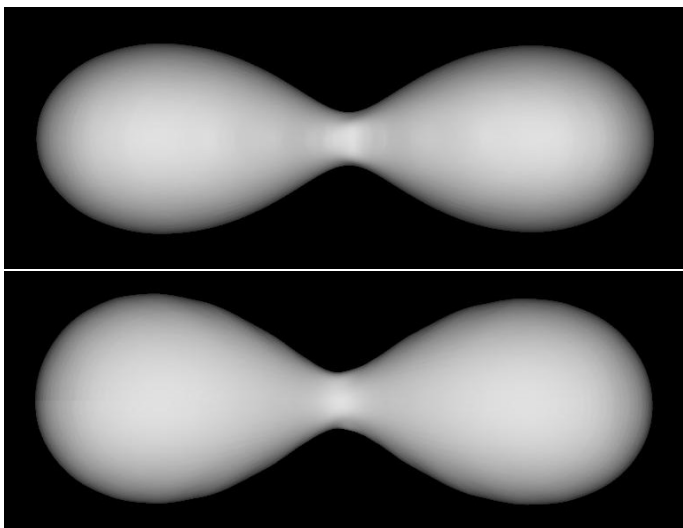


Fig. 4: Shape model of Thymbraeus, see from the equator (top) and the spin axis (bottom).

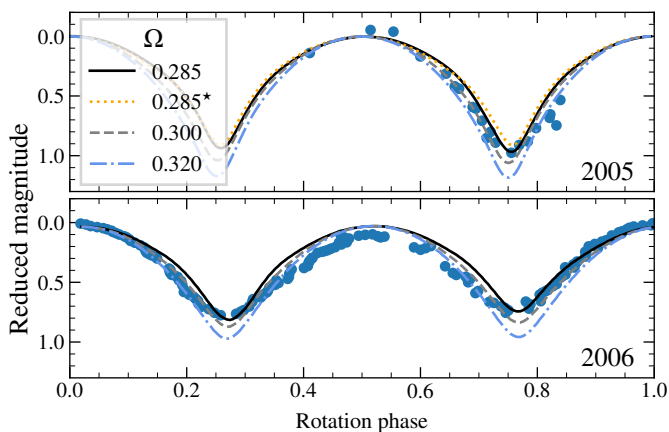


Fig. 5: Effect of Ω on the light curve, compared to the observations of 2005 and 2006 from Mann et al. (2007). The solution marked with a star (\star) does not account for self-shadowing.

ready known from radar imagery to have two lobes at its extremities (Ostro et al., 2000), earning it the nickname of “dog bone”. However, the radar model could not satisfactorily account for the photometric observations which required to take into account the effects of self-shadowing. The stellar occultation observations confirmed that the radar model was not sufficiently elongated and that its central waist was narrower (Descamps et al., 2011). More recently, new high resolution imaging made with the ESO VLT SPHERE/ZIMPOL camera, confirmed that the shape of (216) Kleopatra is very close to an equilibrium dumbbell figure with two lobes and a slightly thicker waist (Marchis et al., 2021) and $\Omega=0.334$, only slightly higher than the value of 0.297 found by Descamps (2015). Consequently, the dumbbell equilibrium figure formalism seems to be a trustworthy approach and our dumbbell model of Thymbraeus appears to be the best suited to explain the photometric light curves.

The presence of two large lobes, separated by a narrower central part, that are roughly identical in size but different in shape is supported by the importance of self-shadowing effects in photometric observations, without which it is impossible to account for the difference in magnitude drop between the minima of some light curves. Such a physical feature is rare and is

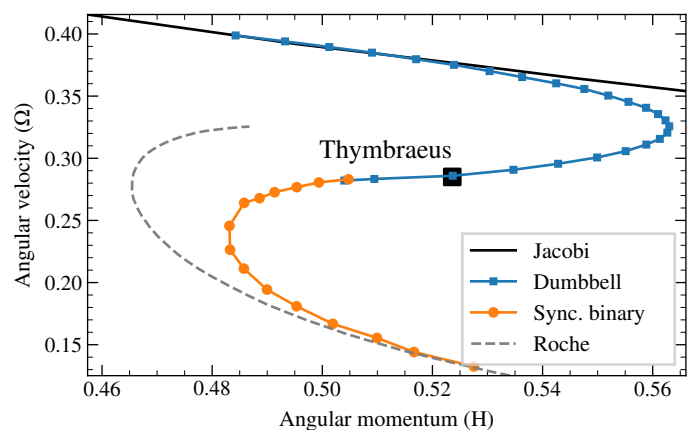


Fig. 6: Angular velocity Ω against angular momentum H for Thymbraeus. The solid curves represent the Jacobi, dumbbell (Descamps, 2015), and twin synchronous binary ellipsoids (Gnat & Sari, 2010) sequences. The Roche approximation is represented by the dashed curve. Figure adapted from Descamps (2015).

a key point to understand the origin and future of this striking shape. It now needs to be confirmed with new high resolution observations either by precision photometry or by stellar occultations. Precision photometry should also allow to discriminate the two pole solutions.

The shape solution found in this work is at the end of the dumbbell equilibrium sequence (Figure 6). The angular momentum H is computed as $\frac{2}{5}\lambda\Omega$, with λ the non-sphericity parameter (Descamps, 2015), equal to 4.5932 for Thymbraeus. This sequence ends for the value $\Omega=0.2815$ and joins at this point the sequence of synchronous congruent binaries numerically investigated by Sharma (2009) and more completely by Gnat & Sari (2010). Furthermore, the bulk density derived from the model is very close to that determined for another Trojan asteroid, (617) Patroclus (Berthier et al., 2020), which is a doubly synchronous system. Should Thymbraeus rotation be accelerated, it would fission and produce a doubly synchronized system.

5. Conclusions

We collected light curves of the Trojan (17365) Thymbraeus in 2015 and 2021, and retrieve observations from 2005, 2006, and 2013. These observations present periodic large-amplitude variations, hinting at the binarity nature of Thymbraeus. We analyze these light curves with the formalism of dumbbell equilibrium figures. We determine Thymbraeus to be a bilobated asteroid, with two lobes of equal size but differing shapes. Its sidereal rotation is found to be 12.672 h, and two symmetric poles corresponding to the direct and prograde rotation are determined at J2000 equatorial coordinates (α_0, δ_0) of $(92^\circ, -77^\circ)$ and $(268^\circ, +77^\circ)$, respectively, with an uncertainty of 2° . The density of Thymbraeus is found to be $830 \pm 50 \text{ kg.m}^{-3}$, confirming the original report by Mann et al. (2007) and similar to that of other Jupiter Trojans and small Kuiper-Belt objects. The rotation of Thymbraeus is close to the end of the dumbbell equilibrium sequence. A faster-rotating Thymbraeus would fission into an equal-size binary reminiscent of (617) Patroclus.

Acknowledgements. We thank the AGORA association which administrates the 60 cm telescope at Les Makes observatory, La Reunion island, under a financial agreement with Paris Observatory. Thanks to A. Peyrot, J.-P. Teng for local support, and A. Klotz for helping with the robotizing.

TRAPPIST-South is funded by the Belgian Fund for Scientific Research (Fond National de la Recherche Scientifique, FNRS) under the grant PDR T.0120.21. TRAPPIST-North is a project funded by the University of Liège, and performed in collaboration with Cadi Ayyad University of Marrakesh. E. Jehin is a Belgian FNRS Senior Research Associate. The authors acknowledge the use of the Virtual Observatory tools *Miriade*³ (Berthier et al., 2008), *SsODNet*⁴ (Berthier et al., 2023), and *TOPCAT*⁵ and *STILTS*⁶ (Taylor, 2005). Thanks to the developers and maintainers.

References

- Bendjoya, P., Abe, L., Rivet, J. P., et al. 2012, in SF2A-2012: Proceedings of the Annual meeting of the French Society of Astronomy and Astrophysics, ed. S. Boissier, P. de Laverny, N. Nardetto, R. Samadi, D. Valls-Gabaud, & H. Wozniak, 643–648
- Benner, L. A. M., Busch, M. W., Giorgini, J. D., Taylor, P. A., & Margot, J. L. 2015, Radar Observations of Near-Earth and Main-Belt Asteroids, 165–182
- Berthier, J., Carry, B., Mahlke, M., & Normand, J. 2023, A&A, 671, A151
- Berthier, J., Descamps, P., Vachier, F., et al. 2020, Icarus, 352, 113990
- Berthier, J., Hestroffer, D., Carry, B., et al. 2008, LPI Contributions, 1405, 8374
- Berthier, J., Vachier, F., Marchis, F., Ďurech, J., & Carry, B. 2014, Icarus, 239, 118
- Brown, M. E., van Dam, M. A., Bouchez, A. H., et al. 2006, ApJ, 639, 4346
- Buie, M., Keeney, B., Levison, H., Olkin, C., & Lucy Occultations Team. 2022, in AAS/Division for Planetary Sciences Meeting Abstracts, Vol. 54, AAS/Division for Planetary Sciences Meeting Abstracts, 512.03
- Carry, B. 2012, Planet. Space Sci., 73, 98
- Carry, B., Hestroffer, D., DeMeo, F., et al. 2011, A&A, 534, A115
- Carry, B., Vachier, F., Berthier, J., et al. 2019, A&A, 623, A132
- Carry, B., Vernazza, P., Vachier, F., et al. 2021, A&A, 650, A129
- Descamps, P. 2015, Icarus, 245, 64
- Descamps, P. 2016, Icarus, 265, 29
- Descamps, P., Marchis, F., Berthier, J., et al. 2011, Icarus, 211, 1022
- Descamps, P., Marchis, F., Michalowski, T., et al. 2007, Icarus, 187, 482
- Eriguchi, Y., Hachisu, I., & Sugimoto, D. 1982, Progress of Theoretical Physics, 67, 1068
- Fraser, W. C., Bannister, M. T., Pike, R. E., et al. 2017, Nature Astronomy, 1, 0088
- Gnat, O. & Sari, R. 2010, ApJ, 719, 1602
- Grundy, W. M., Noll, K. S., Nimmo, F., et al. 2011, Icarus, 213, 678
- Jehin, E., Gillon, M., Queloz, D., et al. 2011, The Messenger, 145, 2
- Johnston, W. R. 2018, NASA Planetary Data System
- Kaasalainen, M., Torppa, J., & Muinonen, K. 2001, Icarus, 153, 37
- Levison, H. F., Olkin, C., Noll, K. S., Marchi, S., & Lucy Team. 2017, in 48th Annual Lunar and Planetary Science Conference, Lunar and Planetary Science Conference, 2025
- Mann, R. K., Jewitt, D., & Lacerda, P. 2007, AJ, 134, 1133
- Marchis, F., Descamps, P., Hestroffer, D., & Berthier, J. 2005, Nature, 436, 822
- Marchis, F., Jorda, L., Vernazza, P., et al. 2021, A&A, 653, A57
- Marchis, F., Wong, M. H., Berthier, J., et al. 2006, IAU Circular, 8732, 1
- Margot, J. L., Nolan, M. C., Benner, L. A. M., et al. 2002, Science, 296, 1445
- Margot, J.-L., Pravec, P., Taylor, P., Carry, B., & Jacobson, S. 2015, Asteroid Systems: Binaries, Triples, and Pairs, ed. P. Michel, F. DeMeo, & W. F. Bottke (Univ. Arizona Press), 355–374
- Merline, W. J., Close, L. M., Dumas, C., et al. 1999, Nature, 401, 565
- Merline, W. J., Close, L. M., Siegler, N., et al. 2001, IAU Circ., 7741, 2
- Morbidelli, A., Levison, H. F., Tsiganis, K., & Gomes, R. 2005, Nature, 435, 462
- Mouis, O., Hueso, R., Beaulieu, J.-P., et al. 2014, Experimental Astronomy, 38, 91
- Muinonen, K. 1998, A&A, 332, 1087
- Muinonen, K. & Lagerros, J. S. V. 1998, A&A, 333, 753
- Nesvorný, D., Vokrouhlický, D., Bottke, W. F., & Levison, H. F. 2018, Nature Astronomy, 2, 878
- Noll, K. S., Brown, M. E., Weaver, H. A., et al. 2020, PSJ, 1, 44
- Noll, K. S., Grundy, W. M., Ryan, E. L., & Benecchi, S. D. 2016, in 47th Annual Lunar and Planetary Science Conference, Lunar and Planetary Science Conference, 2632
- Noll, K. S., Stephens, D. C., Grundy, W. M., & Griffin, I. 2004, Icarus, 172, 402
- Ostro, S. J., Hudson, R. S., Nolan, M. C., et al. 2000, Science, 288, 836
- Pravec, P., Scheirich, P., Kušnirák, P., et al. 2006, Icarus, 181, 63
- Ragozzine, D. & Brown, M. E. 2009, AJ, 137, 4766
- Scheeres, D. J., Britt, D., Carry, B., & Holsapple, K. A. 2015, Asteroid Interiors and Morphology, ed. P. Michel, F. DeMeo, & W. F. Bottke (Univ. Arizona Press), 745–766
- Sharma, I. 2009, Icarus, 200, 636
- Stellingwerf, R. F. 1978, ApJ, 224, 953
- Stephens, R. D., French, L. M., Davitt, C., & Coley, D. R. 2014, Minor Planet Bulletin, 41, 95
- Taylor, M. B. 2005, in Astronomical Society of the Pacific Conference Series, Vol. 347, Astronomical Data Analysis Software and Systems XIV, ed. P. Shopbell, M. Britton, & R. Ebert, 29
- Vachier, F., Carry, B., & Berthier, J. 2022, Icarus, 382, 115013
- Walsh, K. J. & Jacobson, S. A. 2015, Formation and Evolution of Binary Asteroids, ed. P. Michel, F. DeMeo, & W. F. Bottke, 375–393
- Walsh, K. J., Richardson, D. C., & Michel, P. 2008, Nature, 454, 188
- Warner, B. D. 2016, Minor Planet Bulletin, 43, 26
- Yang, B., Hanuš, J., Carry, B., et al. 2020, A&A, 641, A80
- Zhang, Y., Michel, P., Barnouin, O. S., et al. 2022, Nature Communications, 13, 4589

³ *Miriade*: <http://vo.imcce.fr/webservices/miriade/>

⁴ *SsODNet*: <https://ssp.imcce.fr/webservices/ssodnet/>

⁵ *TOPCAT*: <http://www.star.bris.ac.uk/mbt/topcat/>

⁶ *STILTS*: <http://www.star.bris.ac.uk/mbt/stilts/>